Head-on Collisions of Xe Atoms Against Superfluid ^{4}He Nanodroplets

François Coppens, Antonio Leal, Manuel Barranco, Nadine Halberstadt & Marti Pi

ONLINE FIRST

Springer

Springer

CrossMark

Head-on Collisions of Xe Atoms Against Superfluid ^{4}He Nanodroplets

François Coppens^1 · **Antonio Leal^2** ·
Manuel Barranco^2 · **Nadine Halberstadt^1** ·
Marti Pi^2

Abstract We study the head-on collision of a heliophilic xenon atom with a superfluid ^{4}He droplet made of 1000 atoms. At variance with the findings for a heliophobic cesium atom of a similar atomic weight, it is found that the xenon atom has to hit the droplet with a large kinetic energy in order to get across it without being captured. When it is not captured, the xenon impurity does not emerge as a bare atom; instead, due to its heliophilic character it carries away some helium atoms.

1 Introduction

It is well known that helium drops readily capture foreign atoms and molecules [1], and this ability has had a considerable influence on the chemistry and physics of these systems [2]. Among the studies carried out in the past on atom–drop collisions, let us mention those aiming at experimentally determining the density profiles of large ^{4}He and ^{3}He droplets from the scattering of Ar and Kr atoms off helium droplets, which have been analyzed within density functional theory (DFT) [3,4]; the microscopic simulation of the scattering of ^{3}He and ^{4}He atoms from inhomogeneous liquid helium systems [5,6]; and an earlier theoretical work on the scattering of ^{4}He atoms from ^{4}He droplets within a liquid drop plus optical model approach [7].

✉ François Coppens
  francois.coppens@irsamc.ups-tlse.fr

^{1} Laboratoire des Collisions, Agrégats, Réactivité, IRSAMC, UMR 5589, CNRS, Université Toulouse 3, 118 Route de Narbonne, 31062 Toulouse Cedex 09, France

^{2} Departament FQA, Facultat de Física, and IN^{2}UB, Universitat de Barcelona, Diagonal 645, 08028 Barcelona, Spain

🗘 Springer

Very recently, time-dependent density functional theory (TDDFT) has been used to address the capture of Cs or Ne atoms by ^{4}He nanodroplets [8,9]. The Cs capture was treated fully three dimensionally with the Cs atom described as a classical particle, whereas for the Ne capture study the Ne atom was described quantum mechanically, but the description was strictly one dimension.

Motivated by recent experiments that use Xe atoms to visualize vortex arrays in very large helium droplets [10,11], we present here a first step toward the description of the capture of Xe atoms by helium droplets, namely head-on collisions of Xe atoms against a ^{4}He$_{1000}$ droplet. A discussion on the dynamic capture of Xe atoms by droplets hosting vortex lines and vortex arrays will be provided by a forthcoming study combining DFT simulation of vortex arrays as in Refs. [12,13] for helium nanocylinders and nanodroplets and collision with Xe atoms as in this work. Whenever possible, the results for Xe, a heliophilic atom, are contrasted with results for Cs, a heliophobic atom with similar mass.

2 Method and Results

We use the He density functional approach to describe the helium droplet, whereas the Xe atom is treated classically given its large mass. Within TDDFT, we represent the He droplet by a complex effective wave function $\Psi_{He}(\mathbf{r}, t)$ such that the atomic density $\rho(\mathbf{r}, t)$ fulfills $\rho(\mathbf{r}, t) = |\Psi_{He}(\mathbf{r}, t)|^2$; the Xe atom is represented by its classical position $\mathbf{r}_{Xe}(t)$ obeying Newton's equation of motion. We solve the coupled equations

$$i\hbar \frac{\partial}{\partial t} \Psi_{He} = \left[-\frac{\hbar^2}{2m_{He}} \nabla^2 + \frac{\delta \mathcal{E}_{He}}{\delta \rho(\mathbf{r})} + V_X(|\mathbf{r} - \mathbf{r}_{Xe}|) \right] \Psi_{He}$$

$$m_{Xe} \ddot{\mathbf{r}}_{Xe} = -\nabla_{\mathbf{r}_{Xe}} \left[\int d\mathbf{r} \rho(\mathbf{r}) V_X(|\mathbf{r} - \mathbf{r}_{Xe}|) \right] = -\int d\mathbf{r} [\nabla \rho(\mathbf{r})] V_X(|\mathbf{r} - \mathbf{r}_{Xe}|)$$

$$(1)$$

where $\mathcal{E}_{He}$ is the potential energy per unit volume for the functional of Ref. [14] and V_X the Xe–He pair potential taken from Ref. [15]. We refer the reader to Ref. [8] for details on how to solve Eq. (1).

We consider a droplet made of $N = 1000$ helium atoms. Its ground state structure is obtained using DFT and gives a sharp density radius of about 22.2 Å. Then, the dynamics is initiated by placing the Xe atom 32 Å away from the center of mass (COM) of the droplet with an impact parameter equal to zero (head-on collision). The simulations are carried out for initial Xe velocities v_0 ranging from 200 to 600 m/s in the system of reference of the droplet, corresponding to kinetic energies between 315.8 and 2842 K. These energies can be compared to the solvation energy of a Xe atom at the center of a ^{4}He$_{1000}$ droplet, $S_{Xe} = E(Xe@^4He_{1000}) - E(^4He_{1000}) = -316.3$ K. For the sake of comparison, the solvation energy of Cs is -5.2 K and its equilibrium position is in a dimple at the outer droplet surface, about 26.6 Å from its center. Thermal Xe atoms ($v_0 \sim 240$ m/s) are used in the experiments [10,11], and the average drop velocity is about 170 m/s [16].
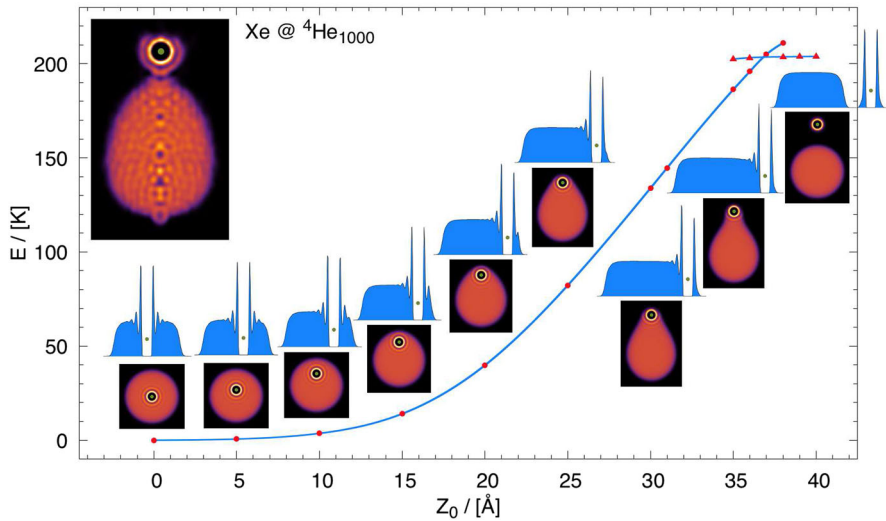
Fig. 1 Energy of the Xe@^{4}He$_{1000}$ complex as a function of the distance between the Xe atom and the COM of the droplet. Several two-dimensional helium densities and density profiles are shown for distances between 0 and 40 Å in 5 Å steps. Connected (*dots*) and disconnected (*triangles*) helium configurations are shown (*see text*). *Top left inset*: snapshot of the helium density at the first turning point during the dynamic evolution of a Xe atom (*green dot*) at $v_0 = 600$ m/s attained 78 ps after it has started (Color figure online)

Figure 1 shows the energy of the Xe@^{4}He$_{1000}$ complex referred to that of the equilibrium configuration (Xe at the center of the droplet, -5716.4 K) as a function of the distance between the Xe atom and the COM of the droplet. It is obtained by a constrained calculation similar to that presented in Ref. [17] for Ba$^+$. With increasing distance, the stretched droplet–Xe configuration eventually breaks into a minicluster around the Xe atom containing about 22 helium atoms disconnected from the rest of the droplet. The appearance of this minicluster is at variance with the situation for a heliophobic impurity such as Cs [8]. The stretched (connected) configuration energies are represented by dots, the disconnected ones by triangles. The two corresponding curves cross at 37 Å. At shorter distances, the connected configuration is stable and the disconnected one metastable, and at larger distances the roles are inverted. In an actual dynamics, the number of He atoms in the minicluster depends on the velocity of the Xe projectile.

Figure 2 displays two-dimensional plots of the helium density for Xe head-on colliding against the ^{4}He$_{1000}$ droplet at $v_0 = 200$ m/s and Fig. 3 the energy of the impinging atom as a function of time, with the corresponding plots for Cs collisions for the sake of comparison. It can be seen that for both species most of the initial kinetic energy is spent in piercing the droplet surface, after which the impurity moves inside the droplet at a velocity well below the critical Landau velocity v_L.

Figure 2 also shows that the collision launches a series of density waves in the droplet that are reflected at the droplet free surface producing complex interference patterns in its bulk. As an illustrative example, Fig. 4 shows the density profile along the incident direction (z axis) corresponding to the Xe collision at $v_0 = 200$ m/s, 6 ps
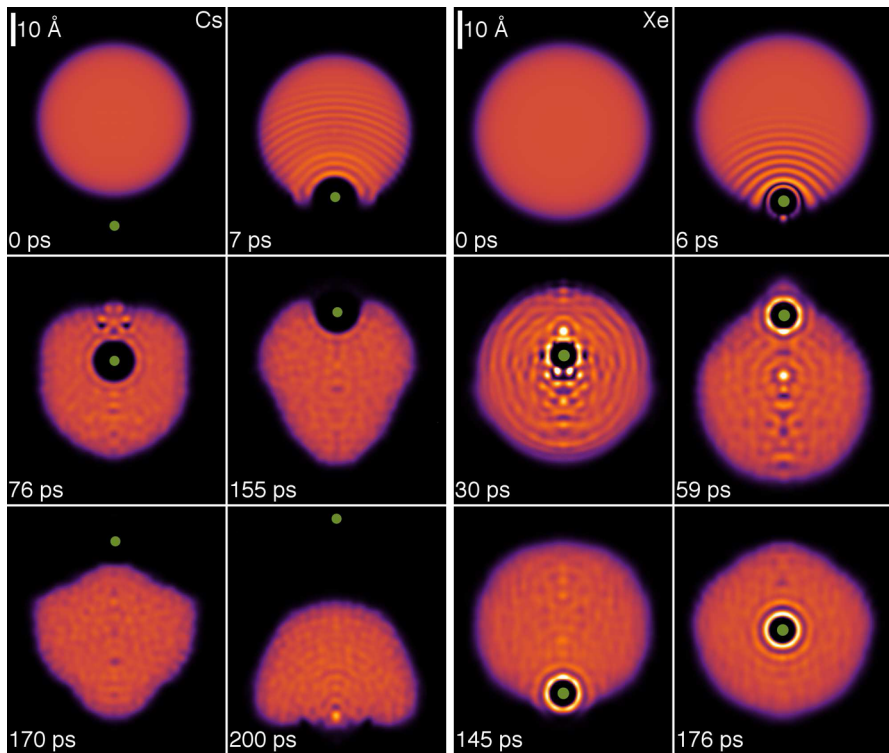
Fig. 2 *Right panel*: dynamic evolution of a Xe atom (*big dot*) approaching the ^{4}He$_{1000}$ droplet from below at $v_0 = 200$ m/s. The corresponding time is indicated in each frame. *Left panel*: same as left figure for a Cs atom (Color figure online)

after the process starts. The wave number associated with this wave can be estimated from the wavelength λ of the oscillations, $q = 2\pi/\lambda \sim 2.7\,\text{Å}^{-1}$.

In the case of Xe, Figs. 2 and 3 reveal the appearance of turning points at which the velocity of the impurity is zero. Note that these points are not fixed during the dynamics since the droplet deforms due to the swift motion of Xe inside it; the droplet is not a rigid object and reacts to the motion of the impurity, with energy being transferred not only from the impurity to the droplet but also the other way around [18].

The top left inset in Fig. 1 shows a snapshot obtained at the first turning point for $v_0 = 600$ m/s, with 57 He atoms around the Xe dopant. We have found that the Xe atom has to hit the droplet at a velocity above 600 m/s in order to go across the helium droplet; otherwise, it remains attached to the droplet. The kinetic energy lost by the Xe atom is partially deposited in the droplet and partially carried away by prompt-emitted helium atoms, i.e., atoms expelled early on in the collision and with a significant kinetic energy. The number of He atoms emitted during the first 78 ps is about 47. For comparison, about 19 atoms are emitted after 185 ps for $v_0 = 200$ m/s. Eventually, the energy deposited into the droplet should be lost by atom evaporation; however, the time scale for this to happen is beyond the reach of any realistic simulation.

The piercing of the droplet by the Cs atom produces a density wave that travels on its surface and collapses at the surface region opposite to the hitting point. This
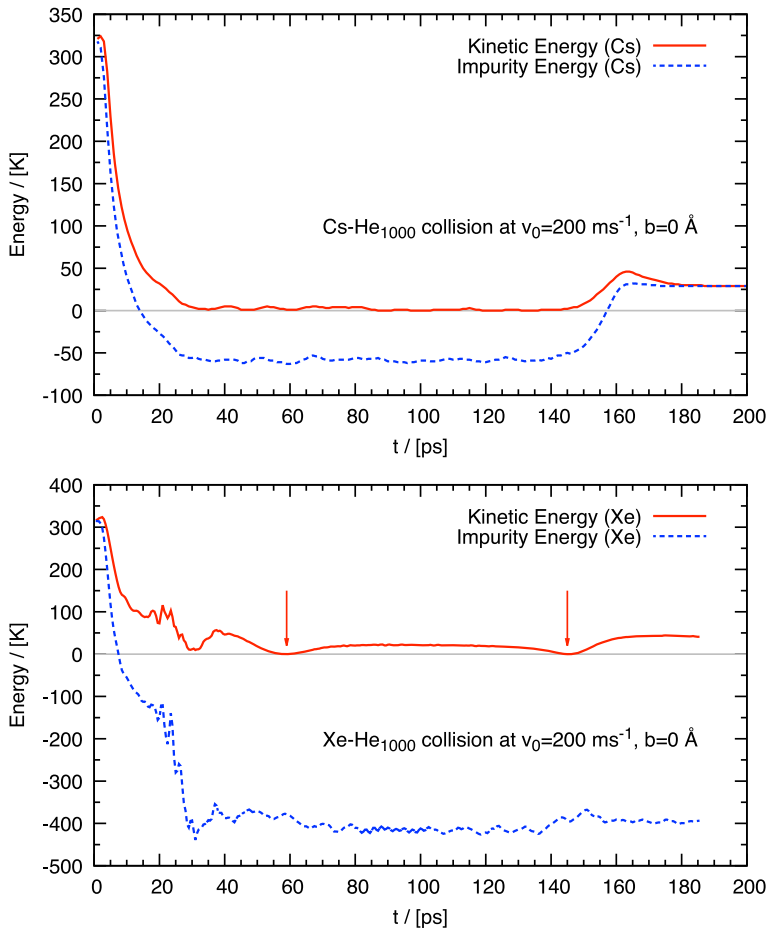
Fig. 3 *Top figure*: kinetic and total (kinetic plus potential) energy as a function of time of a Cs atom head-on colliding against a ^{4}He$_{1000}$ droplet at $v_0 = 200$ m/s. *Bottom figure*: same as top figure for a Xe atom. The *vertical arrows* indicate the first two turning points at 59 and 145 ps, whose corresponding helium densities are shown in the right panel of Fig. 2 (Color figure online)

collapse nucleates a vortex ring (the two dark spots in the 76-ps plot of the left panel of Fig. 2) [8].

It is worth pointing out that the falloff of the Xe velocity in the $t = 20 - 30$-ps interval observed in Fig. 3 is due to the increase in its inertia due to the appearance of a dynamic "snowball"—a crust of helium atoms surrounding the Xe bubble indicated by the bright spots in Fig. 2—that is eventually washed out at larger times. At variance with our findings for Ba$^+$ [18], vortex rings have not been nucleated in the case of Xe; in particular, we have checked that the two dark spots in the 30-ps plot of the right panel of Fig. 2 for Xe do not correspond to a vortex ring.

The collapse of the Cs bubble at the surface of the droplet some 150 ps after the process gives back to the impurity part of the kinetic energy it has lost in the piercing
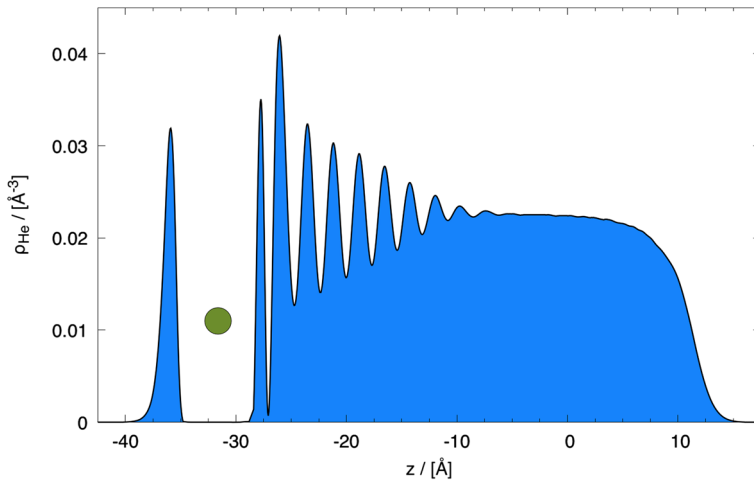
Fig. 4 Density profile of the He_{1000} droplet along the incident direction corresponding to the Xe collision at $v_0 = 200$ m/s after 6 ps (Color figure online)
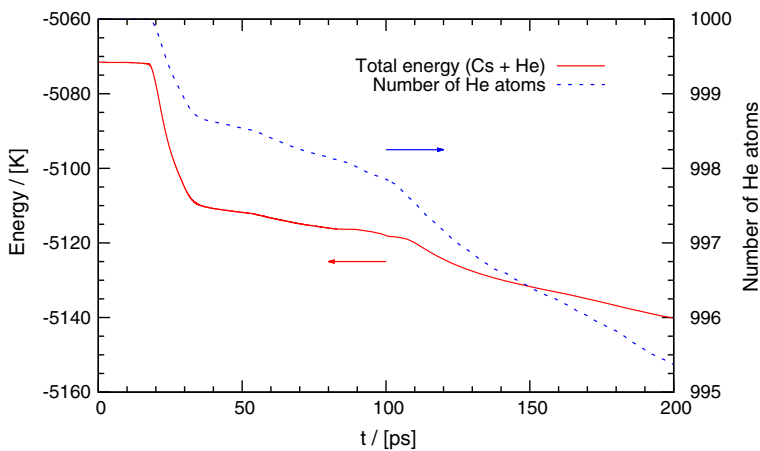

Fig. 5 Total energy (*left scale*) and number of atoms in the droplet (*right scale*) as a function of time for the $Cs@^4He_{1000}$ system at $v_0 = 200$ m/s (Color figure online)

of the droplet. The Cs atom is expelled at 64.5 m/s (corresponding to 33.6 K kinetic energy). The number of prompt-emitted helium atoms is 5, which is smaller than for Xe at the same collision energy (19 atoms). As shown in Fig. 5, they are preferentially emitted as a forward burst (first sharp drop around 20 ps in the number of atoms) and as a backward burst (second sharp drop slightly after 100 ps).

In conclusion, head-on collisions of xenon, a heliophilic atom, involve a kinetic energy exchange of the same order of magnitude as cesium, a heliophobic atom with similar mass. In both cases, this energy is largely dissipated by producing energetic waves in the droplet or it is carried away by promptly emitted helium atoms. The difference is that it takes a much higher velocity for xenon to go through the droplet

and escape than for cesium, as could be expected. Also, density builds up around the xenon during the dynamics, whereas a bubble is created around cesium.

References

1. A. Scheidemann, J.P. Toennies, J.A. Northby, Phys. Rev. Lett **64**, 1899 (1990)
2. J.P. Toennies, A.F. Vilesov, Angew. Chem. Phys. **43**, 2622 (2004)
3. J. Harms, J.P. Toennies, F. Dalfovo, Phys. Rev. B **58**, 3341 (1998)
4. J. Harms, J.P. Toennies, M. Barranco, M. Pi, Phys. Rev. B **63**, 184513 (2001)
5. E. Krotscheck, R.E. Zillich, Eur. Phys. J. D **43**, 113 (2007)
6. E. Krotscheck, R.E. Zillich, Phys. Rev. B **77**, 094507 (2008)
7. D. Eichenauer, A. Scheidemann, J.P. Toennies, Z. Phys. D **8**, 295 (1988)
8. A. Leal, D. Mateo, A. Hernando, M. Pi, M. Barranco, Phys. Chem. Chem. Phys. **16**, 23206 (2014)
9. A. Vilà, M. González, R. Mayol, Phys. Chem. Chem. Phys. **18**, 2006 (2016)
10. L.F. Gomez et al., Science **345**, 906 (2014)
11. C.F. Jones et al., Phys. Rev. B **93**, 180510(R) (2016)
12. F. Ancilotto, M. Pi, M. Barranco, Phys. Rev. B **90**, 174512 (2014)
13. F. Ancilotto, M. Pi, M. Barranco, Phys. Rev. B **91**, 100503(R) (2015)
14. F. Ancilotto, M. Barranco, F. Caupin, R. Mayol, M. Pi, Phys. Rev. B **72**, 214522 (2005)
15. K.T. Tang, J.P. Toennies, Z. Phys. D **1**, 91 (1986)
16. L.F. Gomez, E. Loginov, R. Sliter, A.F. Vilesov, J. Chem. Phys. **135**, 154201 (2011)
17. A. Leal, X. Zhang, M. Barranco, F. Cargnoni, A. Hernando, D. Mateo, M. Mella, M. Drabbels, M. Pi, J. Chem. Phys. **144**, 094302 (2016)
18. D. Mateo, A. Leal, A. Hernando, M. Barranco, M. Pi, F. Cargnoni, M. Mella, X. Zhang, M. Drabbels, J. Chem. Phys. **140**, 131101 (2014)